18th IEEE International Conference on Control Applications
Part of 2009 IEEE Multi-conference on Systems and Control
Saint Petersburg, Russia, July 8-10, 2009

A Multi-Body Approach for 6DOF Modeling of Biomimetic Autonomous Underwater Vehicles with Simulation and Experimental Results

P. Krishnamurthy, F. Khorrami, J. de Leeuw, M. E. Porter, K. Livingston, J. H. Long, Jr.

Abstract— **We propose a six degree-of-freedom multi-body approach for modeling and simulation of Biologically-inspired (or Biomimetic) Autonomous Underwater Vehicles (BAUVs), i.e., artificial fish. The proposed approach is based on considering the BAUV as comprised of multiple rigid bodies interlinked through joints; the external force and torque on each rigid body in the BAUV is expressed using quasi-steady aerodynamic theory and the joint constraints are imposed through an impulse-based technique. A BAUV simulation platform has been implemented based on the proposed modeling framework and has been applied to analyze a specific BAUV inspired by the electric ray. The hardware implementation of the electric ray inspired BAUV is also presented. Finally, sample simulation results and validation against experimental data collected from the electric ray inspired BAUV are also presented.**

I. Introduction

Autonomous Underwater Vehicles (AUVs) have attracted increasing interest [1–3] in recent years due to their potential important role in several civilian and military applications such as intelligence and surveillance applications, search and rescue, mobile communication relays, and hull and pier inspection with object identification and localization. In particular, Biologically-inspired (or Biomimetic) Autonomous Underwater Vehicles (BAUVs), "artificial fish" in particular, are receiving significant attention [4,5] due to the attractive promise of being able to leverage optimizations achieved over millions of years of evolution. The biological study of real fishes and their swimming mechanisms [6,7] offers key design ideas to achieve energy efficiency, stealth, and maneuverability in BAUVs.

Classical approaches to understand the mechanics of how fish swim include the waving plate and the elongated body theories [8,9]. Interest in developing BAUVs has spurred renewed research into various techniques for modeling in recent years [10–26] using primarily approaches based on quasi-steady aerodynamic theory and starting from a focus on modeling of the swimming behavior restricted to single-direction forward swimming on to planar (two translational and one rotational degree of freedom) swimming and, in recent years, to three-dimensional swimming considering also diving (depth change) behavior. Modeling and simulation based on Computational Fluid Dynamics (CFD) approach has also been addressed (for instance, in [27] and references therein); however, a CFD approach is computationally burdensome and does not lend itself to development of a model usable for control design purposes.

The first author is with IntelliTech Microsystems, Inc. (IMI), Bowie, MD, 20715. The second author is with Control/Robotics Research Laboratory (CRRL), Department of Electrical and Computer Engineering, Polytechnic Institute of NYU, Brooklyn, NY, 11201 and with IMI. The third to sixth authors are with Vassar College, Poughkeepsie, NY, 12604. This work was supported in part by the Office of Naval Research (ONR) under contract no. N00014-08-M-0293. Emails: pkrishnamurthy@imicro.biz, khorrami@smart.poly.edu, jodeleeuw@vassar.edu, meporter@vassar.edu, livingst@vassar.edu, jolong@vassar.edu.

In this paper, we address the development of a general multi-body based framework (Section II) for six degree-of-freedom modeling of a general BAUV and the implementation of a simulation and visualization platform (Section III) based on the modeling approach. The dynamic model is developed based on a formulation of a BAUV as the composition of a collection of bodies interlinked through appropriate joints. The hydrodynamic effects on each body are expressed through quasi-steady aerodynamic approximations and the dynamics of the entire BAUV system is attained through the utilization of a impulse-based approach [28,29] for capturing the effects of the joint constraints. The proposed modeling approach is generally applicable to any BAUV with arbitrary arrangements of foils. While prior efforts have typically focused on specific fishes such as the tuna or dolphin, the proposed approach and simulation platform are generic and configurable to a variety of BAUV designs. The proposed approach and simulation platform address full six degree-of-freedom dynamics of the BAUV including roll and pitch motions. The application of the simulation platform to the analysis of the swimming of an electric ray and a ray-inspired BAUV (Section IV) is also presented as well as the validation of simulation results against experimental results (Section V).

II. Modeling

A. Overview of approach

The proposed dynamic modeling technique is based on an articulated multi-body approach (Figure 1), which provides generality and flexibility in terms of support for various fin configurations and designs. Compared to the conventional approach utilized in the robotic fish modeling and control literature wherein the dynamics of the multiple parts of the fish are not modeled explicitly and the cumulative external (hydrodynamic + gravity) force and torque are simply viewed as acting on a rigid body capturing the inertia properties of the entire BAUV, the approach here offers improved fidelity. However, while the approach here is based on a quasi-steady approximation for hydrodynamic effects treating the different parts as hydrodynamically independent, it is to be noted that further fidelity improvements can be attained through a detailed flow modeling including cross-coupling between different parts. In the approach utilized here, the parts of the BAUV that can move relative to each other are modeled as separate rigid bodies and the coupling between the parts is modeled in terms of constraints involving joints of various kinds (hinge, ball-and-socket, slider, etc.). Flexible parts such as the tail and flexible body used in RayBot (Section IV) are approximated as an interconnection of a finite number of bodies. The configuration geometry and parameters of all constituent parts in the multi-body model are specified at run-time through scripts and text-based configuration files as described in Section III.

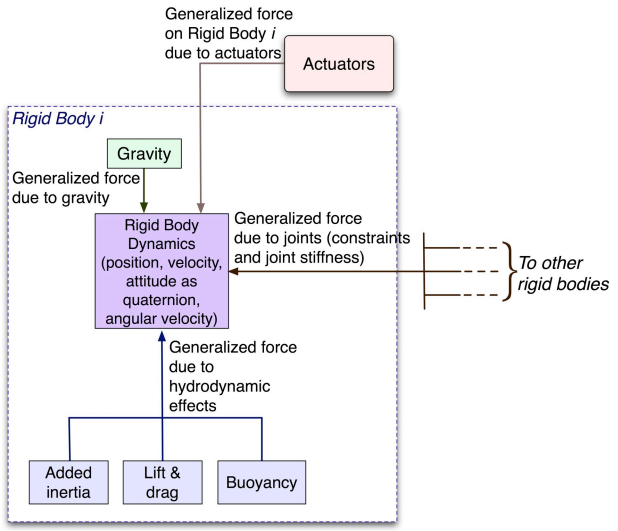

Fig. 1. Conceptual architecture of BAUV multi-body modeling approach.

B. Coordinate frames and rigid body dynamics of each body

Denoting the rigid bodies in the system as $L_1, \ldots, L_N$ where N is the number of rigid bodies in the robotic fish multi-body model, the rigid-body state of each body is comprised of translational position ($p_{t,i}$), rotational position (i.e., attitude) represented as a quaternion ($p_{r,i}$), translational velocity ($v_{t,i}$), and angular velocity ($v_{r,i}$). Each joint in the system typically contributes one state (e.g., a joint angle for a hinge joint). The kinematic reduction of the number of degrees of freedom due to the constraints introduced by the joints linking the bodies in the system is implicitly handled by the impulse-based method for enforcing the joint constraints. A body-fixed frame is introduced for each body L_i as $X_iY_iZ_i$. A suitable inertial frame (denoted as frame 0) is introduced as $X_0Y_0Z_0$ (typically, with Z_0 axis pointing upwards, i.e., aligned opposite to the gravity vector). The rotation matrix which transforms vectors in the body-fixed frame of L_i to the inertial frame is denoted as R_0^i. The translational and angular velocity of each body are represented in a frame fixed to the body (the body frame of L_i). In terms of the 13x1 state vector $[p_{t,i}^T, p_{r,i}^T, v_{t,i}^T, v_{r,i}^T]$ of L_i, the rigid-body dynamics of L_i are written as

$$\dot{p}_{t,i} = R_0^i v_{t,i} \;;\; \dot{p}_{r,i} = \frac{1}{2} p_{r,i} \circ \overline{v}_{r,i} \;;\; M_i\dot{v}_i + C_i(v_i)v_i = \overline{F}_i \quad (1)$$

where the rotation matrix R_0^i is as computed from the quaternion $p_{r,i}$, $\circ$ denotes the quaternion product, $\overline{v}_{r,i}$ is the augmented (with a leading 0) angular velocity vector, $p_i = [p_{t,i}^T, p_{r,i}^T]^T$ is the generalized position vector, $v_i = [v_{t,i}^T, v_{r,i}^T]^T$ is the generalized velocity vector, $\overline{F}_i = [F_i^T, \tau_i^T]^T$ is the generalized force vector (force ad torque combined to yield a 6x1 vector expressed in the body frame of L_i) acting on L_i, and

$$M_i = \begin{bmatrix} m_i I_{3\times 3} & -m_i S(p_{G,i}) \\ m_i S(p_{G,i}) & I_i \end{bmatrix}$$
$$C_i = \begin{bmatrix} m_i S(v_{r,i}) & -m_i S(v_{r,i}) S(p_{G,i}) \\ m_i S(p_{G,i}) S(v_{r,i}) & -S(I_i v_{r,i}) \end{bmatrix} \quad (2)$$

with m_i and I_i being the mass and inertia matrix (expressed in body frame), respectively, of L_i, S denoting the skew symmetric matrix operator, $p_{G,i}$ denoting the position (expressed in body frame) of the center of gravity (CG) of L_i, and $I_{3\times 3}$ denoting the 3x3 identity matrix.

C. External forces and torques

The principal components entering into the generalized 6x1 force vector (force and torque) $\overline{F}_i = [F_i^T, \tau_i^T]$ acting on body L_i are briefly summarized here. Details on the modeling of each of these components and techniques for estimations of various parameters entering therein can be found in the vast literature on aerodynamic and hydrodynamic modeling [30–34] and are only broadly outlined here for brevity. The generalized force $\overline{F}_i$ includes:

- *Gravity:* Generalized force due to gravity is given by $[(f_{G,i}(p_{r,i}))^T, (p_{G,i} \times f_{G,i}(p_{r,i}))^T]^T$ where $f_{G,i}(p_{r,i}) = (R_0^i)^T[0, 0, -mg]^T$, g being acceleration due to gravity.
- *Buoyancy:* The buoyancy force is along the vertical direction (in inertial frame) and through the center of buoyancy CB (whose coordinates in body frame are given by $p_{Bi,}$). The generalized force due to buoyancy is modeled as $[(f_{B,i}(p_i))^T, (p_{B,i} \times f_{B,i}(p_i))^T]^T$ where $f_{B,i}(p_i) = (R_0^i)^T[0, 0, \rho g \nabla_i(p_i)]^T$ with ρ denoting the density of water, $p_{B,i}$ denoting the position (expressed in body frame) of the center of gravity of a body of the same shape as L_i but with uniform density, and $\nabla_i(p_i)$ denoting the volume of water displaced by L_i when the generalized position vector (linear and angular position) are given by p_i. If L_i is completely submerged, then $\nabla_i(p_i)$ is independent of p_i.
- *Added inertia:* The motion of L_i through the fluid results in the application of a generalized force on L_i due to the added mass effects given by $\overline{F}_{A,i} = -M_{A,i}\dot{v}_i - C_{A,i}(v_i)v_i$ where $M_{A,i}$ is a 6x6 symmetric positive-definite matrix and $C_{A,i}$ is the 6x6 matrix obtained from $M_{A,i}$ through the relation

$$C_{A,i}(v_i) = \begin{bmatrix} 0_{3\times 3} & C_{A,i,12}(v_i) \\ C_{A,i,12}(v_i) & C_{A,i,22}(v_i) \end{bmatrix} \quad (3)$$

where $0_{3\times 3}$ is a 3x3 zero matrix, $M_{A,i,kl}$ denotes the $(k,l)^{th}$ 3x3 submatrix of $M_{A,i}$, and

$$C_{A,i,12}(v_i) = -S(M_{A,i,11}v_{t,i} + M_{A,i,12}v_{r,i})$$
$$C_{A,i,22}(v_i) = -S(M_{A,i,21}v_{t,i} + M_{A,i,22}v_{r,i}). \quad (4)$$

The off-diagonal elements of $M_{A,i}$ are typically small and a reasonable approximation for the diagonal elements is to consider the projected area of the body in each direction and estimate the added mass for that direction to be of the form $\frac{\rho\pi a^2 b^2}{6(a+b)}$ where a and b are the principal dimensions of the projected area.
- *Lift and drag:* The net drag arises from various distinct effects including skin friction, vortex shedding, leading edge suction, etc., and can be modeled in a bulk sense to be of the form $D_{H,i}(v_i)v_i$. The lift force on L_i is modeled using standard quasi-steady theory. Denoting the unit vector along the chord (short side of central plane) of L_i by c_{cs} and the unit vector normal to the central plane of L_i by n_{cs}, the unit vector along the span (long side of central plane) of L_i is given by $c_{cs} \times n_{cs}$. The effective lift force on L_i acts at the center of pressure (CP) whose location r_{CP} depends on the geometry of the control surface, but is typically on the central plane around 25% of the chord behind the leading edge. Denoting the relative velocity of CP with respect to the fluid by v_{rel} and decomposing the relative velocity along c_{cs} and n_{cs}, the angle of attack of L_i is obtained as

$$\delta_{\text{attack}} = \text{atan2}\,(v_{av}.n_{cs}/||v_{av}||, v_{av}.c_{cs}/||v_{av}||) \quad (5)$$

where $v_{av} = (v_{rel}^T n_{cs})n_{cs} + (v_{rel}^T c_{cs})c_{cs}$ is the advance velocity. In its simplest form, the generalized force due to the lift on the control surface L_i is modeled as being of the form

$$\overline{F}_{cs} = 0.5\rho A_{cs}|v_{av}|^2[F_l^T, (r_{CP} \times F_l)^T]^T \quad (6)$$
$$F_l = C_N(\delta_{\text{attack}})n_{cs} + C_T(\delta_{\text{attack}})c_{cs} \quad (7)$$

where

$$C_N(\delta_{\text{attack}}) = \begin{cases} C_{N0} \sin\left(\frac{\pi}{2} \frac{\delta_{\text{attack}}}{\delta_{\text{stall}}}\right) \\ \quad \text{for } |\delta_{\text{attack}}| < \delta_{\text{stall}} \\ C_{N0} \text{sign}(\delta_{\text{attack}}) \\ \quad \text{for } |\delta_{\text{attack}}| \geq \delta_{\text{stall}} \end{cases} \quad (8)$$

and a similar model for C_T with C_{T0} instead of C_{N0}. C_{N0} and C_{T0} are parameters depending on the geometry of L_i and δ_{stall} is the stall angle. A_{cs} is a positive coefficient representing the area of the surface of L_i contributing to the lift; A_{cs} could, in general, be a function of the instantaneous configuration (e.g., joint rotations causing stretching of a lifting surface) of the BAUV. C_{N0} and C_{T0} are also, in general, configuration-dependent. The Theodorsen function can be used as in [10] with a linear filter approximation to capture, through a multiplier, the portion of the lift due to the wake of an oscillating foil. The effect of leading edge suction is included similarly through an attitude-dependent quadratic form of the generalized velocity vector. Froude-Kriloff and diffraction forces can also be modeled along similar lines through a generalized force of the form $M_{FKD}(v_{c,i}) + D_{FKD}(v_{c,i})v_{c,i}$ where M_{FKD} and D_{FKD} are 6x6 matrices and $v_{c,i}$ is the fluid velocity vector expressed in the body-fixed frame.

- *Actuators:* Characterizations of the actuation mechanisms (e.g., the tendon mechanism used to actuate the RayBot tail as discussed in Section IV) used to actuate the fins, body flexibility, etc., can be modeled using either static models (i.e., simply as appropriate force and torque models on the relevant bodies in the multi-body system) or dynamic models (i.e., including additional dynamics capturing dynamics of the actuators).

As described above, the hydrodynamic forces and torques on each body in the articulated mechanism are computed based on quasi-steady flow assumption with the different bodies being treated as hydrodynamically independent, i.e., cross-coupling due to wake and backwash are not modeled explicitly; however, these effects are approximately captured through appropriate modifications of the lift and drag coefficients of the bodies. While explicitly accounting for cross-coupling and also incorporating accurate fluid flow models would enhance simulation fidelity at the expense of significantly increased computational complexity and loss of simplicity and tractability for use for control design purposes, the present approach does provide sufficient richness to yield a reasonable match with experimental results (Section V).

D. Impulse-based technique to address joint constraints

The generalized force applied on L_i by the joints connecting L_i to other bodies includes constraint forces and torques as well as effects of joint stiffness (which are modeled by a function of the form $-D_{1,j}\eta_j - D_{2,j}\dot{\eta}_{2,j}$ where η_j and $\dot{\eta}_j$ are the joint variable and its derivative, respectively, and $D_{1,j}$ and $D_{2,j}$ are 6x6 possibly state-dependent matrices). An impulse-based method is utilized to enforce the joint position and velocity constraints. The impulse-based method [28,29] uses an iterative approach to compute a sequence of impulses to apply to the rigid bodies to enforce the constraints and supports general open and closed kinematic chain mechanisms. In the case of a translational joint constraint, the corrective impulses are computed based on the drifts between the two joint points (i.e., the points on each of the linked bodies which are constrained through the joint) while, in the case of a rotational joint constraint, the corrective impulses are computed based on the relative rotation between the two linked bodies. A variety of joints can be modeled as appropriate combinations of translational and rotational joint constraints. For instance, a hinge joint which is most commonly required for BAUV modeling is modeled as a combination of three translational joint constraints (i.e., a spherical joint which eliminates all translational degrees of freedom between the connected bodies) and two rotational joint constraints (i.e., an orientation joint which allows the linked bodies to only rotate around a single common axis). This multi-body formulation with joint constraints allows simulation of general fin, body, and tail motions including flapping, twisting, and undulating motions. The flexibility of the perimeter of the body disc in the electric ray can also be addressed through approximation as a network of multiple discrete fins, thus providing support for modeling a principal distinguishing characteristic of the electric ray, which is a rigid central body disk with a highly flexible perimeter actuated in a distributed fashion.

III. Simulation Platform and Application to a BAUV Inspired by Electric Ray

A BAUV simulation platform has been implemented based on the proposed multi-body modeling approach. The main components in the simulation platform (Figure 2) are:

- Impulse-Based Dynamic Simulation (IBDS): The open-source IBDS library [28,29] provides functionality to set up systems of rigid bodies inter-connected with a variety of joints; the user of the library can then use the provided API to set external forces and torques at each time step and command a simulation update. IBDS utilizes an impulse-based technique to satisfy the joint constraints. A customized version of the IBDS library is used here as the back-end for multi-body computations.
- HydroBody: A generic "hydrodynamic" rigid body has been implemented as a wrapper around IBDS containing the hydrodynamic force and torque computations described earlier. A general set of parameters (including mass, inertia matrix, linear and rotational drag parameters, locations of CG, CB, and CP, lift coefficients, stall angle, etc.) is used to define a HydroBody. Internally, the implementation of HydroBody calls the IBDS API functions to set up appropriate external forces and torques. A Python interface to HydroBody was implemented using SWIG (Simplified Wrapper And Interface Generator) to generate the Python API wrapper code.
- BAUV configuration and simulation control: The geometric and hydrodynamic configuration of the BAUV is set up at run time through the Python scripting interface to HydroBody. This provides a high degree of flexibility since all aspects of fin configuration and parameters as well as time trajectories (and control laws) for fin actuation are set at run time through a Python script and text-based configuration files, thus facilitating easy reconfiguration and testing of BAUV designs.
- Autonomous Vehicle Visualization (AVV): The AVV platform which was implemented in our prior efforts is a general-purpose real-time visualization platform which we have utilized for sea surface vehicle, AUV, and rotorcraft visualizations. Screenshots from AVV applied

to the electric ray inspired BAUV visualization are shown in Figure 3. AVV accepts time-indexed vehicle kinematic data from files or piped (through FIFO files or sockets) to it in real-time from the dynamic simulator; the latter option is utilized in this application with the complete BAUV state vector (including fin and body flexibility states) transmitted to AVV in real-time through a network socket. The standard features provided by the AVV framework include support for arbitrary obstacle geometries (specified through text configuration files at run-time) composed of collections of cuboidal, cylindrical, and ellipsoidal shapes, support for multiple possibly heterogeneous autonomous vehicles, full 3D interaction, keystroke logging and auto-replay, automated screen captures, and export to movie.

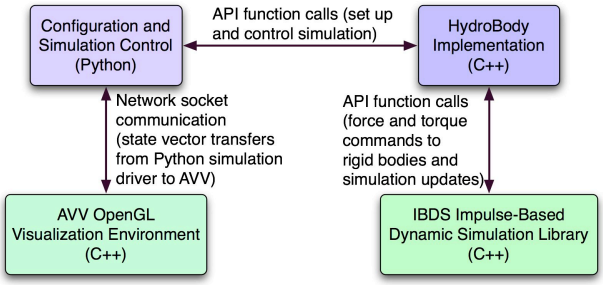

Fig. 2. Architecture of the BAUV simulation platform.

Fig. 3. Screenshots from AVV for BAUV simulation.

IV. RayBot: A BAUV Inspired by the Electric Ray

A BAUV is being implemented based on design concepts inspired by the electric ray, Narcine brasiliensis (Figure 4). Unlike other families of rays, stingrays, and skates, electric rays swim not by undulating the body disc, but rather by oscillating the tail in lateral motion. This allows the body disc to deliver a payload (electric organ) and be used as a lifting body, with the trailing edges and adjacent pelvic fins controlling slot effects. Being negative buoyant, electric rays sink when not actively swimming, and we have evidence that they glide and control the glide under these circumstances, with speed on the glide path inversely proportional to the glide angle (Figure 5). Upon reaching the bottom, the low height profile of the ray provides passive station holding with low induced lift via Bernoulli effect. Our experimental observations and data from the live rays provide key biological inspirations in our design of the RayBot BAUV.

We have implemented a prototype of the "RayBot" skeleton with a biomimetic flexible tail which uses tendon-like actuation with a retinacula-like tendon guide is shown in Figure 6. Experimental results from this prototype and comparison with simulation results are described in Section V. Refinements of the RayBot including an analysis of alternative actuation mechanisms for the tail, pelvic fins, and flexible body disc (including pectoral fins) are being studied in on-going efforts. The RayBot skeleton is housed in a biomimetic body (Figure 8) designed based on a model constructed from a real electric ray. The casted ray is 75 cm long x 50 cm wide, with a maximal height of 15cm at the tip of the caudal fin and disc height of 9 cm. It weighs 5.5 kg, and is easily carried by a single person. Without ballast or payload, the swimming RayBot is slightly buoyant, resting mostly under the water's surface with the very top portion of the body disc exposed. The electronics components are contained within a completely submerged waterproof box accessible from below. The prototype in Figure 8 utilizes a biologically-inspired rack-and-pinion shear actuation mechanism to drive the oscillating, propulsive tail. The servo drives a rack and pinion attached to a fin-ray like skeleton that extends into the tail. The fin-ray skeleton consists of two parallel, elongated, thin PVC plates joined at the distal end; at the proximal and free ends, one plate is attached to the rack and the other to the servo. When the servo translates the rack, the drive plate shears past the anchor plate causing bending of the fin-ray system. To prevent bowstringing and enhance bending, a retinaculum or sheath prevents the two fin rays from separating laterally. The advantage of this fin-ray system is that the actuator can be housed centrally, standard servos can be used, and linkage systems are light and thin.

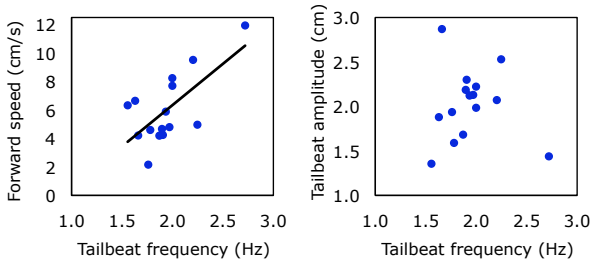

Fig. 4. Observation and performance testing of live electric rays. Bottom two plots show constant-velocity swimming of live electric ray: blue dots are samples from observations of free-swimming juvenile electric rays (three months old); black line in left figure is a linear fit of the observations.

V. Simulation and Experimental Results

The tendon-like mechanism for tail actuation utilized in the RayBot BAUV prototype shown in Figure 6 is easily incorporated in the proposed modeling framework as illustrated in Figure 9. For simplicity, only the central rigid body of the RayBot, the tail (modeled as two bodies interlinked through

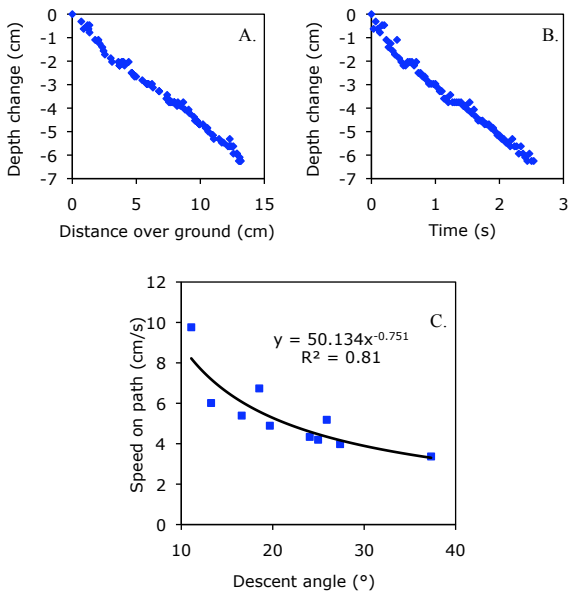

Fig. 5. Gliding behavior of electric ray: A and B. Depth change example in a free-swimming juvenile (three months old); C. Speed as a function of descent angle based on observations from ten trials, with power fit.

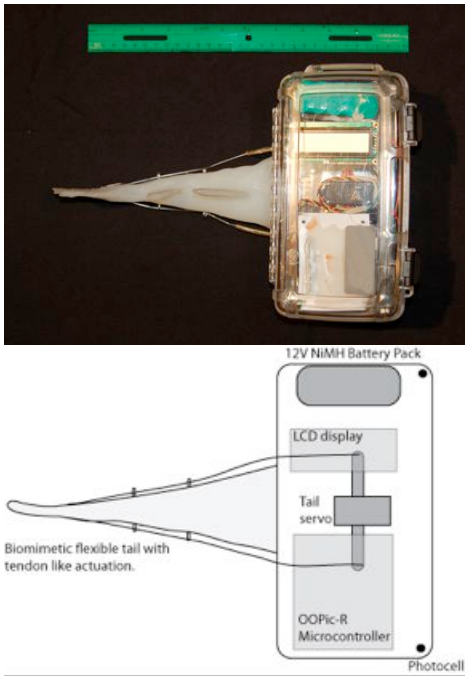

Fig. 6. RayBot experimental prototype with tendon-like actuation of tail.

hinge joints), and the tail actuation mechanism are shown in Figure 9. Models of the tendon-relayed force are used to incorporate appropriate external force and torque inputs into the constituent rigid bodies of the RayBot simulation model. Comparisons between simulation results and experimentally observed data are illustrated in Figure 10 for two key characteristics, tailbeat frequency vs. tailbeat amplitude and tailbeat frequency vs. maximum steady-state forward speed.

For the modeling of the full 6DOF biomimetic RayBot, 9 bodies and 9 hinge joints are used. The body disc is decomposed into a central rigid part and four separately actuated planes in the periphery (corresponding to 4 hinge

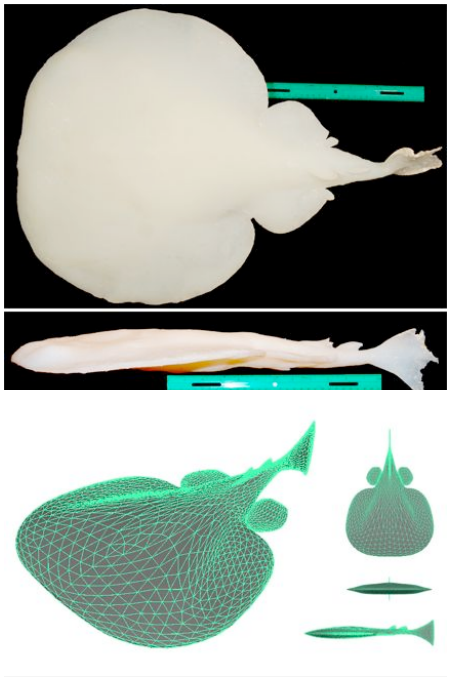

Fig. 7. Design of biomimetic body for RayBot based on measurements from actual electric ray body.

Fig. 8. RayBot experimental prototype in biomimetic body and self-propelled using rack-and-pinion shear actuation of tail.

joints; physically, this is realized through 5 actuated points at the circumference connected as in a wheel spoke with central points). The pelvic fins are separate bodies connected to the central body through hinge joints. The tail is composed of two bodies connected to each other and to the central body through hinge joints. Finally, an additional hinge joint allows bending (nominally with respect to horizontal plane) between the central body plane and the tail bodies (this is primarily exercised in diving behavior of the electric ray). Sample 6DOF simulation results are shown in Figure 11; full state plots are omitted here for brevity.

VI. Concluding Remarks

In this paper, we presented a 6DOF modeling technique and simulation platform for a BAUV based on an impulse-based multi-body approach. In on-going work, we are addressing the further validation of our simulation platform against experimental data from biological and biomimetic rays including experimental data from the RayBot BAUV for turning, roll, and pitch maneuvers and experimental data collected from our live electric rays. The modeling framework and simulation platform also provide a flexible and extensible testbed for analyzing the swimming behaviors of other fishes and BAUV designs in future efforts.

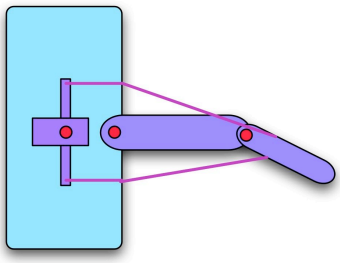

Fig. 9. Modeling of tail actuation using a retinacular-like mechanism, a biologically inspired tendon guide; each red dot is a hinge joint.

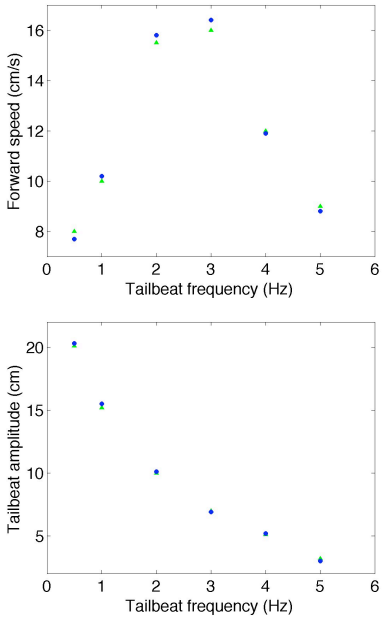

Fig. 10. Comparison of experimental vs. simulation results for forward swimming performance. Top: Tailbeat frequency vs. tailbeat amplitude (Green triangles: experiment, Blue circles: simulation); Bottom: Tailbeat frequency vs. maximum cruising forward speed (Green triangles: experiment, Blue circles: simulation).

REFERENCES

[1] B. Fletcher, "UUV master plan: a vision for navy UUV development," in *Proc. OCEANS 2000 MTS/IEEE Conf. and Exhibition*, Providence, RI, Sept. 2000, pp. 65–71.

[2] G. Griffiths, *Technology and Applications of Autonomous Underwater Vehicles*. CRC Press, 2002.

[3] J. D. Lambert, P. Picarello, and J. E. Manley, "Development of UUV standards, an emerging trend," in *Proc. OCEANS 2006 MTS/IEEE Conf. and Exhibition*, Boston, MA, Sept. 2006, pp. 1–5.

[4] M. S. Triantafyllou, A. H. Techet, and F. S. Hover, "Review of experimental work in biomimetic foils," *IEEE Journal of Oceanic Engineering*, vol. 29, no. 3, pp. 585–594, July 2004.

[5] P. R. Bandyopadhyay, "Trends in biorobotic autonomous undersea vehicles," *IEEE Journal of Oceanic Engineering*, vol. 30, no. 1, pp. 109–139, Jan. 2005.

[6] M. Sfakiotakis, D. M. Lane, and J. B. C. Davies, "Review of fish swimming modes for aquatic locomotion," *IEEE Journal of Oceanic Engineering*, vol. 24, no. 2, pp. 237–252, April 1999.

[7] J. C. Carrier, J. A. Musick, and M. R. H. (Editors), *Biology of Sharks and Their Relatives*. CRC Press, 2004.

[8] M. J. Lighthill, "Note on the swimming of slender sh," *Journal of Fluid Mechanics*, vol. 9, no. 2, pp. 305–317, 1960.

[9] T. Y. Wu, "Swimming of a waving plate," *Journal of Fluid Mechanics*, vol. 10, no. 3, pp. 321–344, 1961.

[10] K. A. Harper, M. D. Berkemeier, and S. Grace, "Modeling the dynamics of spring-driven oscillating-foil propulsion," *IEEE Journal of Oceanic Engineering*, vol. 23, no. 3, pp. 285–296, July 1998.

[11] S. D. Kelly, R. J. Mason, C. T. Anhalt, R. M. Murray, and J. W. Burdick, "Modelling and experimental investigation of carangiform locomotion for control," in *Proc. American Control Conf.*, Philadelphia, PA, June 1998, pp. 1271–1276.

[12] R. J. Mason and J. W. Burdick, "Experiments in carangiform robotic fish locomotion," in *Proc. IEEE Int. Conf. on Robotics and Automation*, San Francisco, CA, April 2000, pp. 428–435.

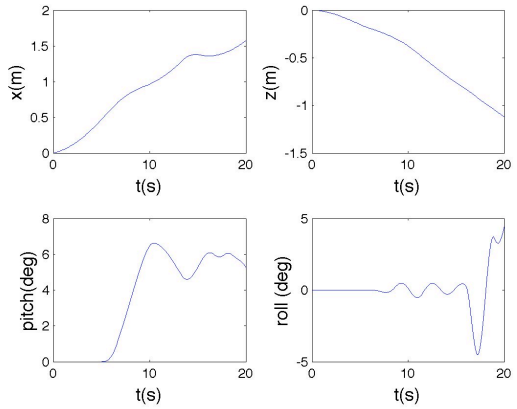

Fig. 11. Sample of 6DOF simulation results of electric ray inspired BAUV.

[13] K. A. Morgansen, V. Duindam, R. J. Mason, J. W. Burdick, and R. M. Murray, "Nonlinear control methods for planar carangiform robot fish locomotion," in *Proc. IEEE Int. Conf. on Robotics and Automation*, Seoul, Korea, May 2001, pp. 427–434.

[14] S. Saimek and P. Y. Li, "Motion planning and control of a swimming machine," in *Proc. American Control Conf.*, Arlington, VA, June 2001, pp. 125–130.

[15] S. D. Kelly and R. B. Hukkeri, "Planar propulsion through the manipulation of circulatory flows," in *Proc. IEEE Conf. on Decision and Control*, Maui, HI, Dec. 2003, pp. 3118–3123.

[16] J. E. Colgate and K. M. Lynch, "Mechanics and control of swimming: A review," *IEEE Journal of Oceanic Engineering*, vol. 29, no. 3, pp. 660–673, July 2004.

[17] S. N. Singh, A. Simha, and R. Mittal, "Biorobotic AUV maneuvering by pectoral fins: Inverse control design based on CFD parameterization," *IEEE Journal of Oceanic Engineering*, vol. 29, no. 3, pp. 777–785, July 2004.

[18] E. Kim and Y. Youm, "Simulation study of fish swimming modes for aquatic robot system," in *Proc. IEEE Int. Conf. on Robotics and Automation*, Barcelona, Spain, April 2005, pp. 3330–3335.

[19] G. Dogangil, E. Ozcicek, and A. Kuzucu, "Modeling, simulation, and development of a robotic dolphin prototype," in *Proc. IEEE Int. Conf. on Mechatronics and Automation*, Niagara Falls, Canada, July 2005, pp. 952–957.

[20] C. Hong and Z. Chang-an, "Modeling the dynamics of biomimetic underwater robot fish," in *Proc. IEEE Int. Conf. on Robotics and Biomimetics*, Hong Kong SAR & Macau SAR, June 2005, pp. 478–483.

[21] P. Giguere, C. Prahacs, and G. Dudek, "Characterization and modeling of rotational responses for an oscillating foil underwater robot," in *Proc. IEEE Int. Conf. on Intelligent Robots and Systems*, Beijing, China, Oct. 2006, pp. 3000–3005.

[22] J. Liu and H. Hu, "A methodology of modelling fish-like swim patterns for robotic fish," in *Proc. IEEE Int. Conf. on Mechatronics and Automation*, Harbin, China, Aug. 2007, pp. 1316–1321.

[23] J. Yu, L. Liu, and M. Tan, "Dynamic modeling of multi-link swimming robot capable of 3-d motion," in *Proc. IEEE Int. Conf. on Mechatronics and Automation*, Harbin, China, Aug. 2007, pp. 1322–1327.

[24] C. Zhou, M. Tan, Z. Cao, S. Wang, D. Creighton, N. Gu, and S. Nahavandi, "Kinematic modeling of a bio-inspired robotic fish," in *Proc. IEEE Int. Conf. on Robotics and Automation*, Pasadena, CA, May 2008, pp. 695–699.

[25] J. Yu, Y. Li, Y. Hu, L. Wang, "Towards development of link-based robotic dolphin: experiences and lessons," in *Proc. IEEE Int. Conf. on Robotics and Biomimetics,* Bangkok, Thailand, Feb. 2009.

[26] R. Ding, J. Yu, Q. Yang, X. Hu, M. Tan, "Platform-level design for a biomimetic amphibious robot," in *Proc. IEEE Int. Conf. on Robotics and Biomimetics,* Bangkok, Thailand, Feb. 2009.

[27] D. Adkins and Y. Y. Yan, "CFD simulation of fish-like body moving in viscous liquid," *Journal of Bionic Engineering*, vol. 3, no. 3, pp. 147–153, Sep. 2006.

[28] J. Bender and A. Schmitt, "Fast dynamic simulation of multi-body systems using impulses," in *Proc. Virtual Reality Interactions and Physical Simulations*, Madrid, Spain, Nov. 2006.

[29] J. Bender, "Impulse-based dynamic simulation in linear time," *Journal of Computer Animation and Virtual Worlds*, 2007.

[30] R. Bhattacharya, *Dynamics of Marine Vehicles*. New York: John Wiley and Sons, 1978.

[31] T. I. Fossen, *Guidance and Control of Ocean Vehicles*. John Wiley and Sons, 1994.

[32] J. Katz and A. Plotkin, *Low-speed aerodynamics*. Cambridge University Press, 2001.

[33] O. M. Faltinsen, *Hydrodynamics of high-speed marine vehicles*. New York: Cambridge University Press, 2005.

[34] P. Krishnamurthy, F. Khorrami, and S. Fujikawa, "A modeling framework for six degree-of-freedom control of unmanned sea surface vehicles," in *Proc. IEEE Conf. on Decision and Control/European Control Conf.*, Seville, Spain, Dec. 2005, pp. 2676–2681.